Cement and Concrete Research 42 (2012) 805–817

Contents lists available at SciVerse ScienceDirect

Cement and Concrete Research

journal homepage: http://ees.elsevier.com/CEMCON/default.asp

Influence of temperature on the hydration products of low pH cements

T.T.H. Bach [a], C. Cau Dit Coumes [a,*], I. Pochard [b], C. Mercier [c], B. Revel [d], A. Nonat [b]

[a] Commissariat à l'Énergie Atomique et aux Énergies Alternatives, DEN/MAR/DTCD/SPDE, BP 17171, 30207 Bagnols-sur-Cèze Cedex, France
[b] ICB, UMR 5209 CNRS Université de Bourgogne, 21078 Dijon, France
[c] LMCPA, Université de Valenciennes et du Hainaut Cambrésis, 59600 Maubeuge, France
[d] Université des Sciences et Technologies de Lille, Centre Commun de Mesures RMN, BP108, 59562 Villeneuve d'Ascq Cedex, France

ARTICLE INFO

Article history:
Received 28 July 2011
Accepted 13 March 2012

Keywords:
Hydration (A)
pH (A)
Temperature (A)
Calcium silicate hydrate (B)
Characterization (B)

ABSTRACT

The chemical evolution of two hydrated "low pH" binders prepared from binary (60% Portland cement + 40% silica fume) or ternary (37.5% Portland cement + 32.5% silica fume + 30% fly-ash) mixtures was characterized over one year at 20 °C, 50 °C, and 80 °C. The main hydrates were Al-substituted C–S–H. Raising the temperature from 20 to 80 °C caused a lengthening and cross-linking of their silicate chains. Ettringite that formed in pastes stored at 20 °C was destabilized. Only traces of calcium sulfate (gypsum and/or anhydrite) reprecipitated after one year in some materials cured at 50 °C and 80 °C. The sulfates released were therefore partially adsorbed on the C–A–S–H and dissolved in the pore solution. The pore solution pH dropped by about 2 units as the temperature increased. Conversely, the soluble alkali fractions did not change significantly. Only the ternary binder resulted in a pore solution pH below 11 at the three temperatures studied.

1. Introduction

Blended cements, obtained by replacing a fraction of Portland cement by pozzolanic minerals (fly-ash, silica fume) or hydraulic minerals (blastfurnace slag), are increasingly used in civil engineering [1] and for nuclear waste conditioning and disposal [2,3]. By recycling byproducts, these additives not only diminish the cost of manufacturing the binders, but also limit CO_2 emissions per metric ton of binder produced, and improve some properties of the resulting cement materials: reduced bleeding, limited heat of hydration, pore refinement, reduced diffusivity and permeability. Moreover, they modify the cement hydration process (kinetics, type of hydrates formed, pore solution chemistry).

Such cements are currently investigated under national or international projects with the objective of specifying materials that could be used in a geological repository for radioactive wastes [4–6]. A range of applications is considered: structural elements, sealing of tunnels, grout for sealing cracks. They all have a common denominator, however: the cement used must have low alkalinity and produce a material with a pore solution pH near 11 (rather than 13.5 for conventional Portland cement, hence the term "low pH cement") to limit its aggressiveness with respect to the repository environment (clay, glass, or spent fuel).

Most studies of low pH cements converge on binary blends of ordinary Portland cement (OPC) and silica fume (SF), and ternary blends of Portland cement, silica fume, and fly-ash (FA) or blast furnace slag (BFS), with a high degree of Portland cement substitution (30 to 70%) [7–12]. Pozzolans are added to consume portlandite—a phase produced by hydration of Portland cement, which would impose an equilibrium pH of 12.5 or more in presence of alkalis. The calcium silicate hydrate formed has a Ca/Si ratio below that in hydrated Portland cement, and this has two advantages: (*i*) the alkali cation concentration in the pore solution can be reduced, as the ability of C-S-H to bind Na^+ and K^+ ions increases when the Ca/Si ratio decreases [13]; (*ii*) the equilibrium pH of the C-S-H decreases with the Ca/Si ratio [14,15].

The mineralogy of hydrated low pH binders has been studied mainly at room temperature by X-ray diffraction and thermogravimetric analysis (Table 1). Low pH cement pastes consist mostly of calcium hydrosilicate highly enriched in silica with small amounts of aluminum. In studies lasting from 90 days to 1 year, they also contain ettringite and residual anhydrous phases. Hydration of binders initially incorporating magnesium-rich blast furnace slag produces a hydrotalcite-type phase. Pastes prepared from binders with the highest silica content (50% OPC + 50% SF, 20% OPC + 50% SF + 30% FA, 20% OPC + 32.5% SF + 47.5% BFS, 60% CEM V + 40% SF) contain no portlandite after 90 days. More diverging results are obtained for a binary binder of 60% OPC + 40% SF, and a ternary binder containing similar fractions of OPC, SF and FA. In the first case, Lothenbach [16] reported for instance the transient precipitation of portlandite between 1 and 14 days (with a maximum at 4 days), whereas Garcia et al. [12] and Codina et al. [11] continued to observe this phase after 90 days and 1 year, respectively. The long-term persistence of portlandite in some materials can be attributed to poor dispersion of silica fume; Codina [11] noted the presence of a large number of residual silica fume agglomerates in the pastes. Moreover, when the same binder is used to prepare concrete, shearing due to the aggregates during mixing improves the dispersion of the silica fume, and portlandite is consumed more rapidly [17].

* Corresponding author. Tel.: +33 4 66 39 74 50; fax: +33 4 66 33 90 37.
E-mail address: celine.cau-dit-coumes@cea.fr (C.C.D. Coumes).

0008-8846/$ – see front matter © 2012 Elsevier Ltd. All rights reserved.
doi:10.1016/j.cemconres.2012.03.009

Table 1
Composition of low pH cement pastes.

Binder composition	Type of material	Phases observed	Pore solution pH	Reference
60% OPC–40% SF	Cement paste (W/B = 0.5 cured in sealed bag at 20 ± 1 °C)	After 1 year: C-A-S-H (Ca/Si = 1.5), portlandite (2%), ettringite, calcite, C_2S, C_3S, hematite, quartz	12.2	[11]
	Cement paste (W/B = 0.5 cured at 98% RH at 21 ± 2 °C)	After 90 days: C-A-S-H (Ca/Si = 0.8–1.2), portlandite (2.6%), ettringite, calcite, C_2S, C_3S, C_4AF, quartz	12.2	[12]
	Cement paste (W/B = 0.8)	After 1 year: C-A-S-H (Ca/Si = 0.9), ettringite, C_2S, C_3S, calcite	11.3	[16]
50% OPC–50% SF	Cement paste (W/B = 0.5 cured at 98% RH at 21 ± 2 °C)	After 90 days: C-A-S-H (Ca/Si = 0.8–1.2), ettringite, calcite, C_2S, C_3S, C_4AF, quartz	11.2	[12]
37.5% OPC–32.5% SF–30% FA	Cement paste (W/B = 0.5 cured in sealed bag at 20 ± 1 °C)	After 1 year: C-A-S-H (Ca/Si = 1.2), ettringite, calcite, C_2S, C_3S, hematite, mullite, quartz, magnetite	11.7	[11]
35% OPC–35% SF–30% FA	Cement paste (W/B = 0.5 cured at 98% RH at 21 ± 2 °C)	After 90 days: C-A-S-H (Ca/Si = 0.8–1.2), portlandite (1.6%) ettringite, C_2S, C_3S, C_4AF	11.6	[12]
20% OPC–50% SF–30% FA	Cement paste (W/B = 0.5 cured at 98% RH at 21 ± 2)°C	After 90 days: C-A-S-H (Ca/Si = 0.8–1.2), ettringite, C_2S, C_3S, C_4AF	10.5	[12]
37.5% OPC–32.5% SF–30% BFS	Cement paste (W/B = 0.5 cured in sealed bag at 20 ± 1 °C)	After 1 year: C-A-S-H, portlandite, ettringite, hydrotalcite, calcite, C_2S, C_3S	12.2	[11]
20% OPC–32.5% SF–47.5% BFS	Cement paste (W/B = 0.5 cured in sealed bag at 20 ± 1 °C)	After 1 year: C-A-S-H (Ca/Si = 1.0, Al/Si = 0.07), ettringite, hydrotalcite, calcite, C_2S, C_3S	11.7	[11]
60% CEM V[a]–40% SF	Cement paste (W/B = 0.5 cured in sealed bag at 20 ± 1 °C)	After 1 year: C-A-S-H, ettringite, hydrotalcite, calcite, C_2S, C_3S, quartz, mullite	12.1	[11]

[a] Comprising 55% OPC clinker, 22% BFS and 22% FA.

Using ^{29}Si-MAS NMR, Lothenbach [16] estimated the rate of silica fume consumption by pozzolanic reaction in a paste comprising 60% OPC and 40% SF. Silica fume was consumed at a high rate during the first two months, but much more slowly thereafter. The residual silica fraction was about 40% after one year.

Low pH cement pastes have a pore solution pH at least one unit lower than in specimens of OPC or cements containing blast furnace slag and fly-ash, and the pH varies little after 90 days [11,12]. The differences between the values reported in the literature for the same formulation are attributable to different degrees of pozzolanic reaction progress in the materials due to the variable dispersion of silica fume. The pore solutions are all characterized by a strong reduction in their sodium and potassium concentrations (between 1 and 5 mmol/L) compared with Portland cement (70 to 90 mmol/L) [11,18]. In addition, the potassium fraction retained by the hydrated binders is greater by a factor of about 4 than for sodium ions.

All these studies were carried out at room temperature. In some areas of a geological repository, however, cement materials could be exposed to temperatures of up to 80 °C [19]. This article describes a study of the chemical evolution of two low pH binders (prepared from a binary blend of OPC and SF, and a ternary blend of OPC, SF, and FA) when hydrated at 50 °C or 80 °C.

2. Experimental data

2.1. Raw materials

Table 2 shows the chemical composition and properties of the raw materials used in the formulation of low pH binders. Portland cement was selected for its low alkali content. It was rich in tricalcium silicate and depleted in aluminates (73% C_3S, 11% C_2S, 4% C_3A, 6% C_4AF, and 3% gypsum). Silica fume comprised more than 96% amorphous silica. Using a mechanically densified form was a tradeoff between the required reactivity and ease of implementation. The aluminosilicate fly-ash corresponded to class V according to European standard EN 197-1.

2.2. Low pH cement pastes

Two low pH binders were investigated in this work: (*i*) a binary binder, B40, comprising 60% OPC and 40% SF; (*ii*) a ternary binder, T1, with 37.5% OPC, 32.5% SF, and 30% FA.

To improve the dispersion of silica fume in the paste, the binder constituents were ground together in a planetary ball mill (Retsch PM400 mixer-mill: 250 rpm, 150 g of material and 50 g of 10 mm diameter stainless steel balls in a 250 mL grinding jar, particle size distribution after grinding : $d_{10} = 2$ μm, $d_{50} = 11$ μm, $d_{90} = 31$ μm). The cement pastes (water/binder (W/B) mass ratio = 0.55) were blended in a standard mortar mixer (per European standard EN 196-1) according to the following sequence: (*i*) pour water into mixer bowl, (*ii*) add dry filler while stirring at low speed, (*iii*) mix at low speed for 3 min, then at high speed for 3 min.

Twenty-four samples were prepared for each formulation. They were stored in hermetically sealed 50 mL polypropylene containers and submitted to three types of curing: (*i*) in a controlled-environment chamber at 20 °C with 95% relative humidity, (*ii*) in an oven at 50 °C, (*iii*) in an oven at 80 °C. To prevent drying, the samples were placed in water-filled boxes. Curing was initiated 30 min after mixing.

2.3. Material characterization

2.3.1. Characterization of solids

Both test formulations were characterized after 3, 6, and 12 months of hydration. The protocol adopted for the 3-month characterization consisted of three steps: (*i*) quenching the materials in liquid nitrogen on removal from the oven to freeze the mineralogical state formed above room temperature; (*ii*) fragmentation of the sample to centimeter scale, followed by quenching again in liquid nitrogen; (*iii*) sublimation of the ice in a freeze drier until constant sample weight was obtained.

However, this protocol had a major drawback: freeze-drying resulted in dehydration of ettringite [20] and suppression of its X-ray diffraction signal. The second and third steps in the method for terminating hydration were therefore modified for the 6- (T1) and 12-month (T1 and B40) paste samples: after quenching (to avoid any phase assemblage rearrangement which may occur during slow cooling), the samples were ground into very fine fragments and then rinsed 5 times in isopropanol, which was eliminated by drying the samples at room temperature in a desiccator with 23% relative humidity maintained by a saturated solution of potassium acetate. This value was chosen both to avoid water absorption by the samples and to limit water loss from ettringite.

Table 2
Characteristics of binder constituents.

		CEM I	Silica fume	Fly-ash
Chemical composition (wt.%)	CaO	66.90	0.50	5.10
	SiO_2	22.00	96.30	51.50
	Al_2O_3	3.30	<0.20	25.20
	Fe_2O_3	2.74	0.10	5.80
	MgO	0.60	<0.20	1.80
	MnO	<0.02	0.02	0.06
	Na_2O	<0.20	<0.20	0.40
	K_2O	<0.05	0.34	1.33
	$Na_2O + K_2O$	<0.25	0.34<<0.54	1.73
	TiO_2	0.18	<0.05	1.31
	P_2O_5	0.24	0.09	0.98
	Sulfides	<0.10	<0.10	<0.10
	Sulfates	2.40	0.24	0.66
	Loss on ignition (1000 °C)	2.02	2.21	4.78
Mean particle diameter (μm)[a]		$d_{10} = 3.2$ $d_{50} = 16.6$ $d_{90} = 49.5$	$d_{10} = 5.0$ $d_{50} = 18.0$ $d_{90} = 46.1$	$d_{10} = 3.0$ $d_{50} = 24.2$ $d_{90} = 136.1$
Specific surface area (m^2/g)[b]		1.3	23.0	2.2
Phases observed by X-ray diffraction[c]		C_3S (+++) C_2S (+++) Brownmillerite (+) C_3A (+) Gypsum (+) Anhydrite (+) Calcite (+)	Cristobalite (+++) Quartz (++) Maghemite (++) Silicon (+) Silicon oxide (+)	Quartz (+++) Mullite (++) CaO (+) Maghemite (+)

[a] Grain size distribution determined by laser particle size analysis (powder dispersed in absolute ethanol).
[b] Specific surface area measured using the BET method by nitrogen adsorption.
[c] Intensity of main diffraction peak: + + + strong, + + moderate, + weak.

After grinding to a particle size below 80 μm, the mineralogy of the cement pastes was characterized by X-ray diffraction (Siemens D8, copper anode, $\lambda_{K\alpha1} = 1.54056$ Å, 40 mA and 40 kV, scanning from $2\theta = 5°$ to 60° in 0.017° steps, 50 s measurement time per step). Thermogravimetric analysis of the powder was also performed under nitrogen atmosphere on 50 ± 2 mg samples (Netzsch TGA/DSC STA409 PC, 10 °C/min heating rate from 30 to 1000 °C). The Ca/Si and Al/Si ratios in the hydrates were determined by X-ray microanalysis on polished cross sections observed with a scanning electron microscope (Philips XL30, 15 kV acceleration voltage, EDX PGT detector, calibrated on alumina and wollastonite, statistics on 80 measurement points).

Additional characterizations were performed by ^{27}Al MAS NMR and by ^{29}Si MAS NMR on the 6-month old ground cement pastes. The tilt angles were π/6 and π/2 respectively. The ^{27}Al MAS spectra were recorded at a Larmor frequency of 208.5 MHz using a Bruker Avance II 800 MHz (18.8 T) spectrometer. The spectra were made up of 2048 free induction decays with a pulse length of 1 μs and a relaxation delay of 1 s to ensure quantitative reliability of the intensities observed for the ^{27}Al central transition for sites experiencing different quadrupole couplings. The samples were spun at 24 kHz in 3.2 mm probe, and the chemical shifts were referenced to $Al(H_2O)_6^{3+}$. The ^{29}Si MAS spectra were recorded at a Larmor frequency of 79.5 MHz using a Bruker Avance 400 MHz (9.4 T) spectrometer. The spectra were obtained with 256 scans (pulse length of 5 μs and optimized relaxation delay of 120 s). The samples were spun at 5 kHz in a 7 mm probe, and the chemical shifts were referenced to trimethysilylsilane (TMS). Spectral decomposition was performed with DMFit software [21].

2.3.2. Characterization of pore solutions

The pore solution pH in the low pH materials was estimated by the suspension method, which is much easier to implement than extraction of the pore solution under high pressure [22]. It has been shown that in low pH materials, the pH of the pore solution is controlled by the equilibrium dissolution of C-S-H [11]. The dilution during preparation of the suspension was insufficient to desaturate the solution with respect to this phase and the measured pH was representative of the pore solution. Conversely, with Portland cement paste, the alkali ions present at high concentrations in the pore solution are involved in controlling the pH, and the dilution induced by preparing the suspension results in a decrease in the measured pH.

A cement suspension was prepared with ultrapure water (decarbonated by boiling for 1 h, then cooling in a stream of nitrogen) and cement paste ground to a particle size below 80 μm (5 g of solid in 45 mL of water). The pH was determined after 24 h of stirring under inert atmosphere (N_2) at the initial sample curing temperature (20, 50 or 80 °C). The high alkalinity measurement electrode was first calibrated at the same temperature with buffer solutions: borate (pH 9.23 at 20 °C, 9.01 at 50 °C, and 8.88 at 80 °C), carbonate (pH 10.06 at 20 °C, 9.83 at 50 °C, and 9.73 at 80 °C) and calcium hydroxide (pH 12.63 at 20 °C, 11.71 at 50 °C, and 10.99 at 80 °C). The suspension was then filtered at the test temperature and the filtrate was acidified. Its composition was analyzed by ICP-AES (Vista Pro Varian, Ca, Si, Al, S, Na, K standardization with matrix reconstitution).

3. Results and discussion

3.1. Effect of temperature on the mineralogy of cement pastes

3.1.1. X-ray diffraction

The diffraction patterns of the cement pastes stored at 20 °C, 50 °C, and 80 °C are compared in Fig. 1 (B40) and Fig. 2 (T1) after 12 months of curing. Similar results were obtained at earlier age, after 3 and 6 months of curing. The samples consisted mainly of calcium hydrosilicate; no portlandite was detected. Raising the temperature resulted in slightly lower intensity of the C_2S reflections (especially at 80 °C), which could indicate greater reaction progress. It had no effect on the reflections of C-S-H. No well crystallized calcium hydrosilicate was identified, even at 80 °C. This result is consistent with observations performed on Portland cement paste at 85 °C [23]. It is in contradiction, however, with data obtained with synthetic phases showing that storing C-S-H with a Ca/Si ratio of 0.85 for 145 days at 85 °C results in crystallization of tobermorite, while C-S-H with Ca/Si ratios of 1.1 and 1.4

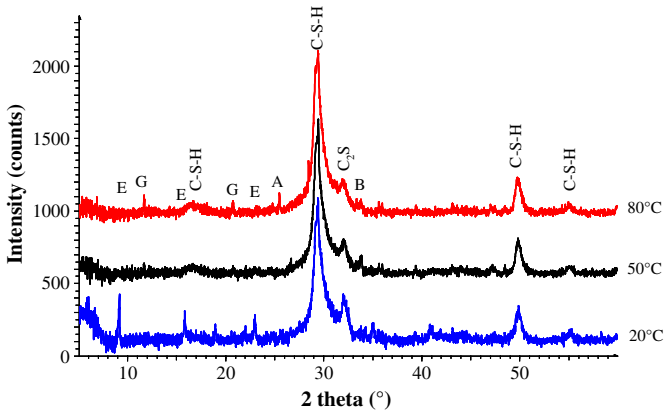

Fig. 1. Effect of temperature on the mineralogy of B40 paste after 12 months of curing (E = ettringite, C-S-H = calcium hydrosilicate, C_2S = belite, B = brownmillerite $C_2(A, F)$, G = gypsum, A = anhydrite).

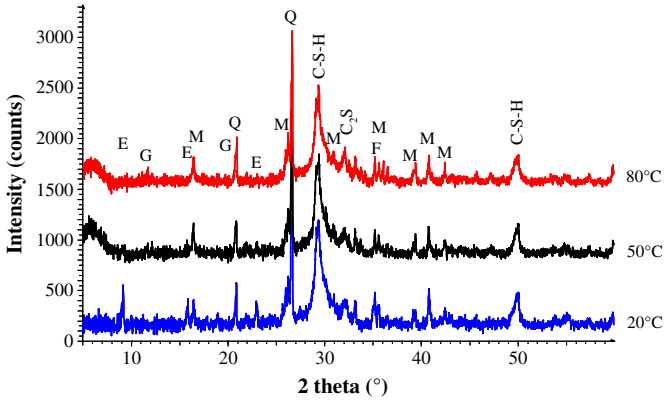

Fig. 2. Effect of temperature on the mineralogy of T1 paste after 12 months of curing (E = ettringite, M = mullite, Q = quartz, C-S-H = calcium hydrosilicate, C_2S = belite, F = hematite, G = gypsum).

lead to the formation of jennite, and C-S-H with a Ca/Si ratio of 1.8 results in the precipitation of afwillite [24]. For samples that were not freeze-dried (T1 paste after 6 and 12 months, B40 paste after 12 months), the disappearance of ettringite was observed above 50 °C; this can be explained by the fact that the stability range of ettringite decreases with temperature in favor of calcium monosulfoaluminate hydrate [25,26]. No new sulfate phase was detected in the samples stored at 50 °C and 80 °C after 3 and 6 months. After one year of conservation, however, the diffractogram for B40 paste showed low-intensity peaks characteristic of gypsum ($2\theta = 11.6°$ and 20.7° observed at 50 °C and 80 °C) and anhydrite ($2\theta = 25.5°$ observed at 80 °C). In the case of T1 paste, only gypsum was detected at 80 °C. Moreover, non reactive anhydrous fly-ash phases (mullite, quartz, hematite) were detected at all temperatures as expected. Glasser et al. [24] investigated the hydration of binders rich in fly-ash (40% OPC 40% and 60% FA) at 55 and 85 °C, and reported the formation of zeolites (thomsonite, phillipsite). Such compounds were not observed in T1 paste after up to one year.

Increasing the curing time from 3 to 12 months did not result in any significant change in the sample mineralogy, except for the precipitation of calcium sulfate in the samples stored at 50 and 80 °C.

3.1.2. X-ray microanalysis

The Ca/Si and Al/Si molar ratios in the cement paste hydrates were estimated by EDS analysis on polished cross sections prepared from 6-month old samples. To take into account the local heterogeneity of the materials, 80 measurements were carried out per sample on different zones, avoiding the residual anhydrous phases (Figs. 3 to 5).

For B40 paste cured at 20 °C (Fig. 4), the Al/Si ratio was relatively invariable at 0.04 ± 0.01, a value near the initial Al/Si ratio of the anhydrous binder (0.046). Aluminum appeared to be mainly inserted in the C-A-S-H (Fig. 3). The Ca/Si ratio exhibited greater dispersion. The distribution mode occurred at 0.85 ± 0.05 (for an initial Ca/Si ratio of 0.84 in the anhydrous binder), but a significant number of analyses gave much lower values—as low as 0.3. EDS mapping of silicon showed the presence of unreacted or partially reacted silica fume agglomerates (Fig. 6). Therefore, the low Ca/Si measurements probably originated from the existence of a submicronic mixture of C–A–S–H and residual silica.

The results for the ternary binder stored at 20 °C were more dispersed (Fig. 5). The distribution modes for the Ca/Si and Al/Si ratios were 0.75 ± 0.05 and 0.07 ± 0.01, respectively. These values are respectively higher and lower than for the anhydrous binder (Ca/Si = 0.52 and Al/Si = 0.19), which can be attributed to a large unreacted fly-ash fraction. Within the hydrated phases, aluminum was mostly incorporated in the C-A-S-H (Fig. 3).

For both cement pastes, raising the curing temperature from 20 to 80 °C produced silica enrichment in the C-A-S-H, which resulted in a slight decrease in the Ca/Si ratio and a more significant drop in the Al/Si ratio. Under these conditions, the pozzolanic reaction exhibited greater progress. The dispersion of results was also reduced, which could indicate greater homogeneity of the hydrates.

3.1.3. Thermogravimetric analysis

Bound water could be compared from one sample to another only when identical protocols were used to stop hydration. Regardless of

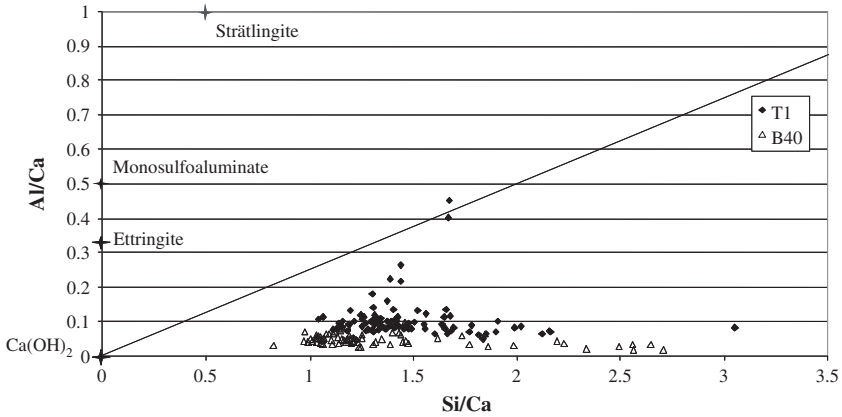

Fig. 3. X-ray microanalysis results for B40 and T1 pastes after 6 months of curing at 20 °C versus Si/Ca and Al/Ca ratios. The straight line passing through coordinates (0, 0) and (2, 0.5) is the Al/Si ratio limit of 0.25 observed in the C-A-S-H [44].

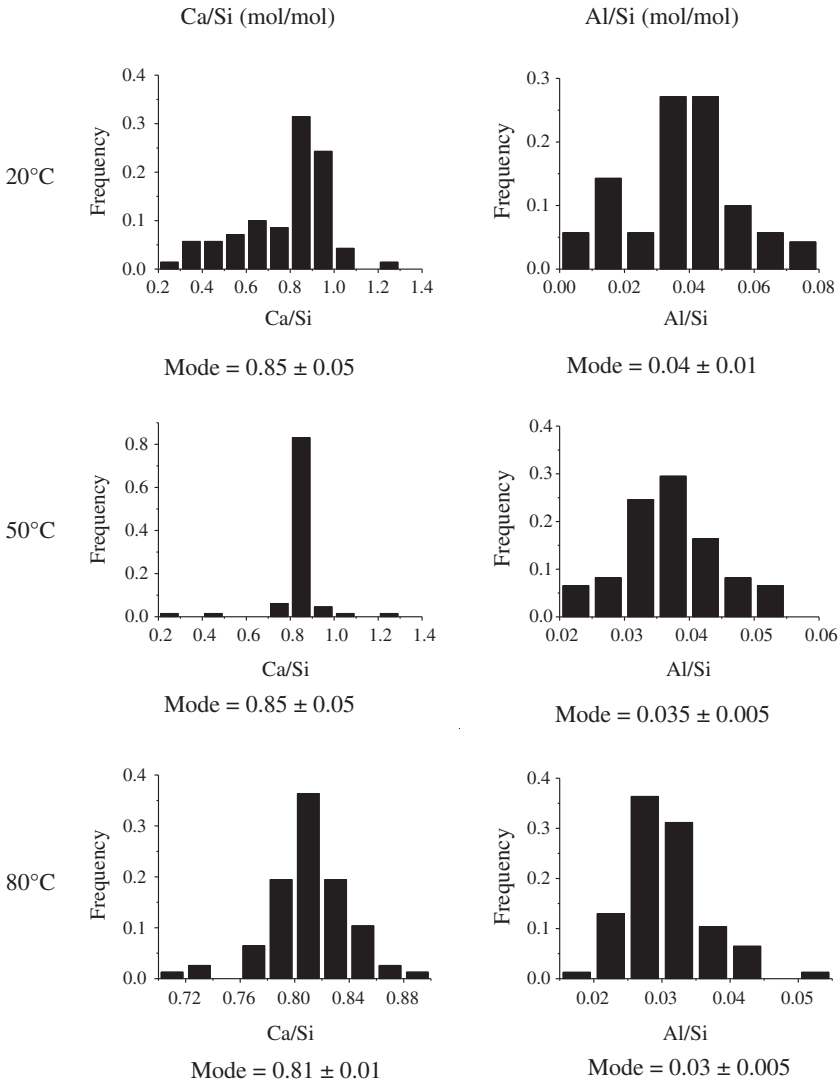

Fig. 4. Ca/Si and Al/Si ratios measured by X-ray microanalysis in the hydrates of B40 paste (cured for 6 months).

the curing temperature, the bound water fraction increased steadily between 3 and 6 months in B40 paste, and between 6 and 12 months in T1 paste (Fig. 7). Hydration continued throughout these periods, although no significant mineralogical evolution was observed.

For any given formulation, the bound water fraction appeared to decrease slightly as the temperature increased (except for the B40 binder after 3 months). This result seems to be in contradiction with the hypothesis that hydration progressed with temperature, unless the C-S-H formed at 50 or 80 °C contained less water than those precipitated at 20 °C. This was actually showed by Odler and Skalny [27] who investigated hydration of tricalcium silicate at elevated temperature (50, 75 and 100 °C). With increasing temperature, the H/S ratio of the C–S–H decreased.

3.1.4. NMR

The previous characterizations have shown that C-A-S-H constitutes the main hydrate in low pH materials. X-ray diffraction is not well adapted for its characterization because of its nanocrystalline properties. The C-S-H peaks in the diffractograms of Figs. 1 and 2 are broad, poorly resolved, and show no evolution with the sample curing temperature. In Portland cement and blended (OPC + fly-ash) cement, higher temperatures are known to modify the C-S-H structure by lengthening the silicate chains [28–31]. High-resolution magic-angle spinning NMR is one of the few tools providing information on the local structure of C-S-H [32–42]. B40 and T1 pastes were therefore characterized by ^{27}Al and ^{29}Si MAS NMR after 6 months of curing at 20 °C, 50 °C and 80 °C.

3.1.4.1. ^{27}Al MAS NMR. The naturally abundant ^{27}Al nucleus (spin 5/2) has a high gyromagnetic ratio, making it suitable for detection by NMR. However, analysis of ^{27}Al MAS NMR spectra is complicated by quadrupolar broadening, which can result in overlapping resonance peaks when several sites are present. The resolution was enhanced by using a strong magnetic field and a high rotational speed. Therefore, we will use the peak maxima for discussion.

The main information derived from the chemical shift of aluminum concerns the coordination number. It is possible to discriminate between tetrahedral environments (shifts between 50 and 100 ppm), pentahedral environments (25 to 40 ppm), and octahedral environments (−10 to 20 ppm) (Table 3). ^{27}Al NMR spectroscopy has been widely used to investigate the Al insertion into C–S–H [32–34,37,41–45]. Related ^{27}Al NMR spectra may exhibit various resonances from Al in IV-, V- and VI-fold oxygen coordination. Three types of aluminum incorporation in the tetrahedra of the dreierketten silicate chain have been reported: an Al[Q_3] bridging site across the interlayer [42] or between two dreierketten chains adjacent to the same calcium oxide plane [45], an Al[Q_{2p}] bridging site charge-balanced by interlayer Ca^{2+}, and an Al[Q_2] paired site [45] (sketch in Fig. 8). Three Al[VI] resonances have been described

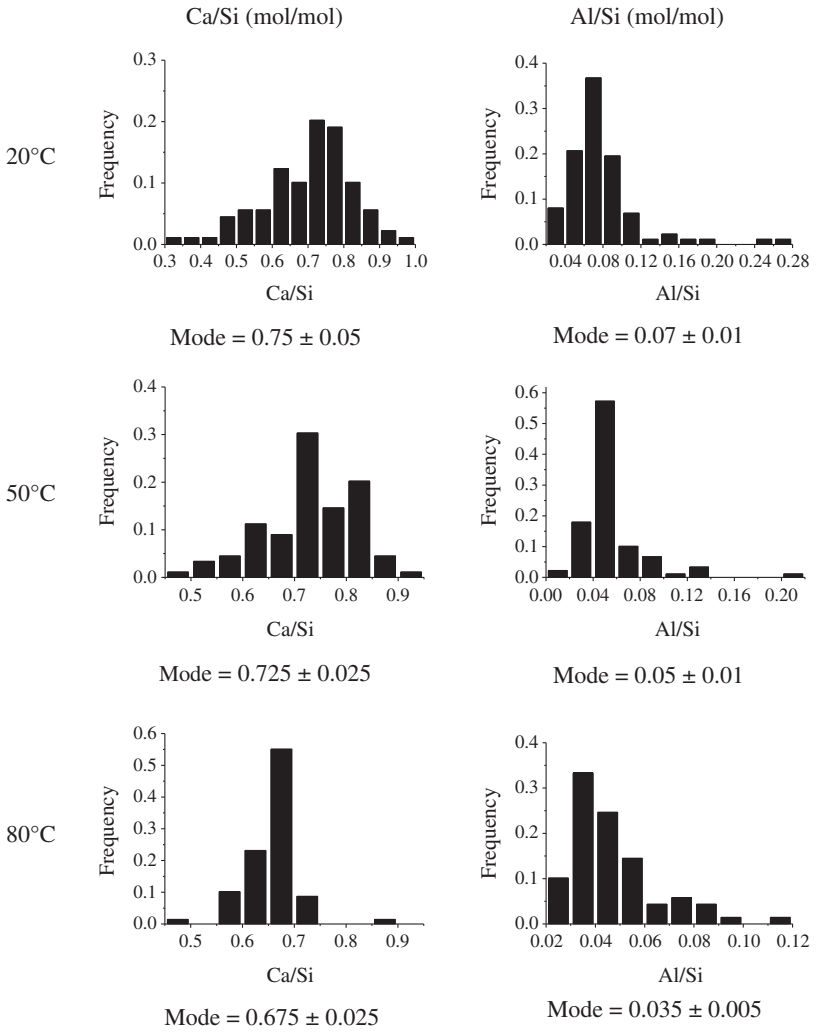

Fig. 5. Ca/Si and Al/Si ratios measured by X-ray microanalysis in the hydrates of T1 paste (cured for 6 months).

in hydrated Portland cement: $\delta \approx 13$ ppm for ettringite, $\delta \approx 11$ ppm for AFm phases, $\delta \approx 5$ ppm related to C–A–S–H formation. Three main assumptions have been postulated to assign this latter resonance: it may correspond to an amorphous aluminate hydrate, designated TAH [34], to insertion of octahedral aluminum in the interlayer space of C–S–H to compensate for negative charges of the main layers [42], or to adsorption on the boarder of the C–S–H particles [45]. It has been shown recently [45] that there seems to be no relationship between the amount of Al[V] and Al[VI] and the charge to compensate on the C–S–H main layers, which contradicts the second assumption. In this article, the third hypothesis was considered in a first approach, meaning that Al[VI] was attributed to C–A–S–H for mass balance.

• B40 paste: The spectra for B40 paste are shown in Fig. 9a. Although the samples were freeze-dried prior to characterization, a sharp peak corresponding to ettringite was noticed for a chemical shift of 13.2 ppm. According to Skoblinskaya and Krasilinov [46,47], the decomposition of ettringite in vacuum occurs in four discrete stages. Initially, zeolitic water is lost, the water content decreasing from 32 H_2O to ~30 H_2O per formula unit. In stages 2 and 3, water bonded to calcium is lost in two stages, decreasing from ~30 H_2O to ~18 H_2O, and subsequently to ~6 H_2O. The ettringite structure seems to collapse during this third stage and becomes X-ray amorphous. Zhou et al. [48] investigated more carefully the structure of metta-ettringite, the dehydroxylated product containing 11–13 H_2O per formula unit, and concluded that the columns $[Ca_3Al(OH)_6]^{3+}$ are preserved but, as intercolumnar water is lost, individual columns move closer together and order at long distance is lost. Freeze-drying thus strongly affected the X-ray diffraction pattern of ettringite but, the local environment of aluminium atoms in the columns being preserved, this mineral could still be detected by ^{27}Al-MAS NMR.

The disappearance of ettringite was obvious for curing temperatures of 50 and 80 °C, and a component was clearly observed for a chemical shift of 10.1 ppm in the samples stored at 20 and 50 °C. Such a shift is characteristic of aluminum at an octahedral site in an AFm phase [49]. This type of phase was not detected by X-ray diffraction, because of its very low content and/or its poor crystallinity. B40 paste thus appeared to contain small quantities of an AFm phase, perhaps hemicarboaluminate due to incipient carbonation, or to the cement carbonates reaction. Hemicarboaluminate is unstable above 50 °C [50], which could account for its disappearance in the sample stored at 80 °C.

Spectral decomposition was performed. In ettringite, aluminum occurs in a highly symmetrical sixfold coordination. It experiences no electrical field gradient and no quadrupolar effect, and the corresponding lineshape used was a simple Lorentzian. The Czjzek model has been shown to be applicable to quadrupolar nuclei with a coordination at least equal to four in a wide range of disordered materials. In particular, it was successfully applied to ^{27}Al NMR spectra of calcium monosulfoaluminate hydrate and TAH [51]. We thus used this model for spectral decomposition of asymmetric peaks related to Al[V], Al[VI], and in some cases to Al[IV]. Fig. 9b, for example, shows a simulated 6-component spectrum for B40 paste cured at 20 °C and Table 4

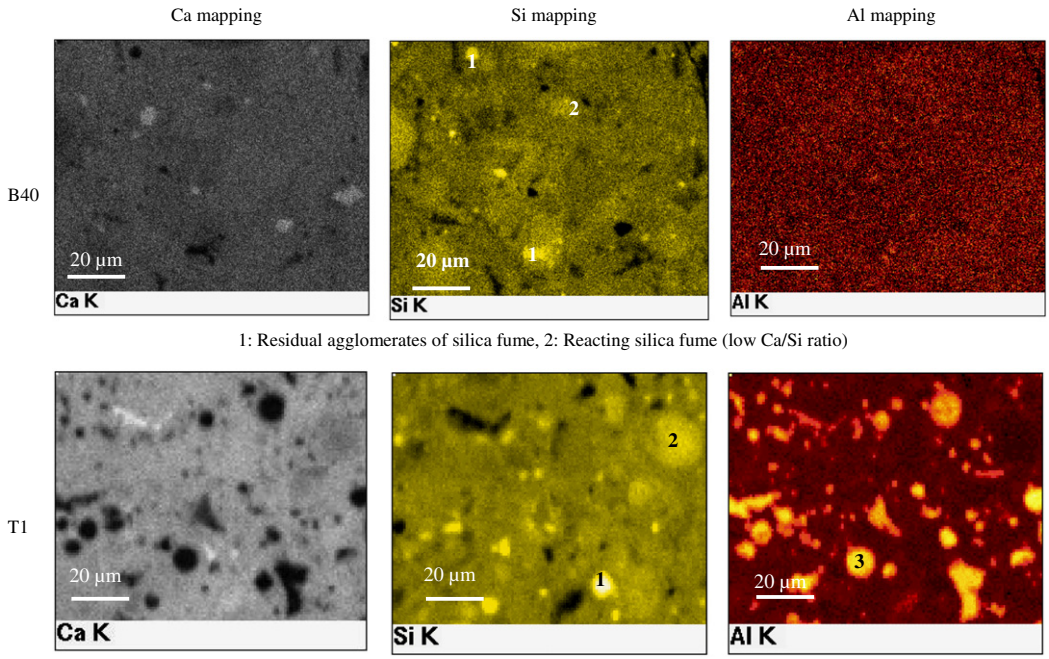

Fig. 6. Elemental mapping of B40 and T1 pastes after 6 months of curing at 20 °C.

summarizes the distribution of the aluminum sites versus temperature. As previously explained, we assumed in a first approach that Al[VI], which was closely associated with C–A–S–H, could be attributed to this hydrate for mass balance.

In the C-A-S-H, raising the curing temperature slightly increased the aluminum fraction at Q_{2p} or Q_3 sites, which was offset by smaller aluminum fractions at pentahedral sites. The peak recorded for chemical shifts between 58.2 ppm and 64.6 ppm (Al Q_{2p} and/or Q_3 site) could be correctly fitted by a Gaussian distribution for the sample stored at 20 °C, but included two asymmetric components (at 64.4–64.6 ppm and 57.1–57.9 ppm) for samples stored at higher temperatures.

• T1 paste: Analysis of the spectra for T1 paste was complicated by the superimposed resonance peaks of fly-ash and cement hydrates (Fig. 10), and only qualitative analysis was performed. Ettringite was partially destabilized by curing at 50 °C, and completely at 80 °C. At all three curing temperatures, the samples contained an AFm phase that had not previously been identified by X-ray diffraction. The resonance peaks of ettringite and the AFm phase were 3 ppm higher than in the reference data, which could be due to the presence of iron (supplied by fly-ash) in these compounds.

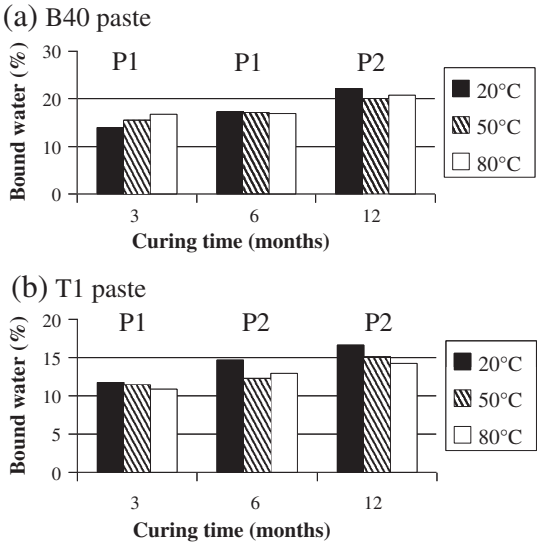

Fig. 7. Effect of curing time and temperature on bound water fraction in B40 (a) and T1 (b) cement pastes. P1 and P2 refer to the protocol used to stop hydration: either freeze-drying (P1), or soaking in isopropanol (P2).

3.1.4.2. ^{29}Si MAS NMR. The ^{29}Si nucleus (spin 1/2) exhibits very low natural abundance (4.7%), with a low gyromagnetic ratio γ. It therefore has low NMR sensitivity. In addition, its relatively long relaxation time (up to several hundred seconds in some cases) required long recording times (about 9 h) to obtain a usable signal/noise ratio. The chemical shifts for silicates in the solid phase ranged between −60 and −120 ppm compared with TMS. This range can be subdivided according to the degree of connectivity of the silicate tetrahedra [52]. In C-A-S-H, the chemical shifts of silicates with first-neighbor aluminates are modified by:

- a 3 to 5 ppm increase in the chemical shift of a silicate with one neighboring aluminate, designated $Q_n(1Al)$,
- a 10 ppm increase in the chemical shift of a silicate with two neighboring aluminates, designated $Q_n(2Al)$.

Fig. 8 summarizes locations of silicates observed by Pardal et al. [45] and the corresponding chemical shifts. The overlapping resonance peaks for adjacent chemical shifts make it difficult to identify the silicate sites without a clear idea of the short-range material structure. Spectral decomposition constraints were thus added by assuming the C-A-S-H model as described in Fig. 8, in which tetrahedral aluminum is substituted for silicates at Q_2, Q_{2p} and Q_3 sites (all quantities are in percentages).

(i) The dreierketten structure of C-A-S-H silicate chains requires:

$$Q_{2p} + Q_{2p}(1Al) + Q_3 + Q_3(1Al) = 1/2[Q_2 + Q_2(1Al)] \quad (1)$$

(ii) Each Si at a $Q_{2p}(1Al)$ site has an Al neighbor substituted for Si at a Q_2 site.

$$Q_{2p}(1Al)\% = Al(IV) \text{ at a } Q_2 \text{site} \quad (2)$$

Table 3
Chemical shifts (δ), asymmetry parameters (η) and quadrupolar coupling constants (C_Q) of aluminum in cement phases investigated by ^{27}Al-MAS NMR.

Phase	Coordination number	Chemical shift	Reference
Alite, belite	Al[IV]	Al[IV] $\delta_{iso} = 86$ ppm	[65]
		Al[IV] $\delta^{cg}_{1/2-1/2} \approx 86$ ppm with $B_0 = 14.1$ T	[34]
C_3A	Al[IV]	Al(1): $\delta_{iso} = 79.5 \pm 0.5$ ppm, $C_Q = 8.69 \pm 0.05$ MHz, $\eta = 0.32 \pm 0.02$	[49]
		Al(2) :$\delta_{iso} = 78.3 \pm 0.5$ ppm, $C_Q = 9.30 \pm 0.05$ MHz, $\eta = 0.54 \pm 0.02$	
		$\delta^{cg}_{1/2-1/2} \approx 81$ ppm, Al in an impure form in C_3A with $B_0 = 14.1$ T	[34]
		Al_1 : $\delta_{iso} = 81.4$ ppm, $C_Q = 8.9$ MHz, $\eta = 0.32$ (50%)	[66]
		Al_2 : $\delta_{iso} = 81$ ppm, $C_Q = 9.5$ MHz, $\eta = 0.56$ (50%)	
		Al_1 : $\delta_{iso} = 86$ ppm $C_Q = 8.7$ MHz $\eta = 0.3$ (43%)	[67]
		Al_2 :$\delta_{iso} = 88$ ppm $C_Q = 8$ MHz $\eta = 0$ (57%)	
C–A–S–H	Al[IV]	Al[IV] at Q_2 or Al[IV] at Q_{2p} compensated by Al[V] or Al[VI] between layers : $\delta^{cg}_{1/2-1/2} \approx 74$ ppm with Bo = 17.5 T	[42]
		$\delta_{iso} = 74.6$ ppm $C_Q = 4.5$ MHz or $\delta^{cg}_{1/2-1/2} \approx 72$ ppm with $B_0 = 14.1$ T	[33]
		$\delta^{cg}_{1/2-1/2} \approx 70$ to 73.7 ppm, with $B_0 = 9.4$ T	[68]
		$\delta^{cg}_{1/2-1/2} \approx 70$ ppm, with $B_0 = 7.05$ T	[69]
		$\delta^{cg}_{1/2-1/2} \approx 71$ ppm, with $B_0 = 19.6$ T	[70]
		$\delta_{iso} = 74$ ppm $C_Q = 3.7$ MHz $\eta = 0.6$	[66]
		$\delta_{iso} = 60$–67 ppm—Al[IV] in Q_{2p} site with charge compensation by Ca^{2+} between layers and Al[IV] in Q_3 site	[45]
	Al[V]	$\delta_{iso} = 33$ ppm low intensity	[45]
		$\delta^{cg}_{1/2-1/2} \approx 35$ ppm with $B_0 = 14.1$ T	[34]
		$\delta_{iso} = 38.5$ ppm,	[37]
		$\delta^{cg}_{1/2-1/2} \approx 30$ ppm with $B_0 = 7.05$ T	[69]
		$\delta_{iso} = 39.9$ ppm $C_Q = 5.1$ MHz or $\delta^{cg}_{1/2-1/2} \approx 33.5$ ppm with $B_0 = 14.1$ T	[33]
	Al[VI]	$\delta_{iso} = 3.5$ ppm	[45]
Mullite	Al[IV]	$\delta^{cg}_{1/2-1/2} \approx 56$ ppm with $B_0 = 7.05$ T	[56]
	Al[VI]	$\delta^{cg}_{1/2-1/2} \approx -2$ ppm with $B_0 = 7.05$ T	[56]
Ettringite	Al[VI]	$\delta_{iso} = 13.1 \pm 0.1$ ppm, $C_Q = 0.360 \pm 0.010$ MHz, $\eta = 0.19 \pm 0.03$	[49]
		$\delta_{iso} = 13.2$ ppm	[51]
		$\delta_{iso} = 13$ ppm, $C_Q = 1.8$ MHz, $\eta = 0.6$	[66]
Silicated katoite	Al[VI]	δ_{iso} ~12 ppm (main signal), and δ_{iso} ~4 ppm (lower intensity)	[67]
Calcium monosulfoaluminate hydrate or other AFm phases (e.g. Friedel's salt or C_4AH_{13})	Al[VI]	$\delta_{iso} = 11.8 \pm 0.2$, $C_Q = 1.7 \pm 0.2$ MHz	[49]
		$\delta = 10.3$ ppm, asymmetric peak, Czjzek model	[51]
		$\delta^{cg}_{1/2-1/2} \approx 9.5$ ppm with $B_0 = 14.1$ T	[34]
γ-AH_3	Al[VI]	Al(1) $\delta_{iso} = 8.1$ ppm (main signal) and $\delta_{iso} = -1.6$ ppm (lower signal)	[67]
Amorphous aluminum hydroxide (TAH) or calcium aluminate hydrate produced as a separated phase or as a nanostructure precipitate on the C-S-H surface	Al[VI]	$\delta_{iso} = 5 \pm 0.1$ ppm $C_Q = 1.13$ MHz Degradation at about 70–90 °C	[34]
		$\delta_{iso} = 6.5$ ppm, asymmetric peak, Czjzek model	[51]

(iii) Each Al substituted for Si at a bridging site (Q_{2p} or Q_3) has two Si neighbors at a Q_2(1Al) site, and each Al substituted for Si at Q_2 has a Q_2(1Al) neighbor.

$$Q_2(1Al)\% = 2\,Al(IV)\text{at a bridging site} + 1\ Al(IV)\ \text{at a}\ Q_2\ \text{site} \quad (3)$$

Given the quantities of aluminum and silicon in B40 paste, the silicon fractions at Q_{2p}(1Al) and Q_2(1Al) sites could be inferred from the aluminum NMR results (Table 5). Q_{2p}(1Al) sites accounted for less than 1%, and were not taken into account in the remainder of the study. Finally, the possible variation range for chemical shifts related to each type of site was bounded on the basis of published findings (Fig. 8).

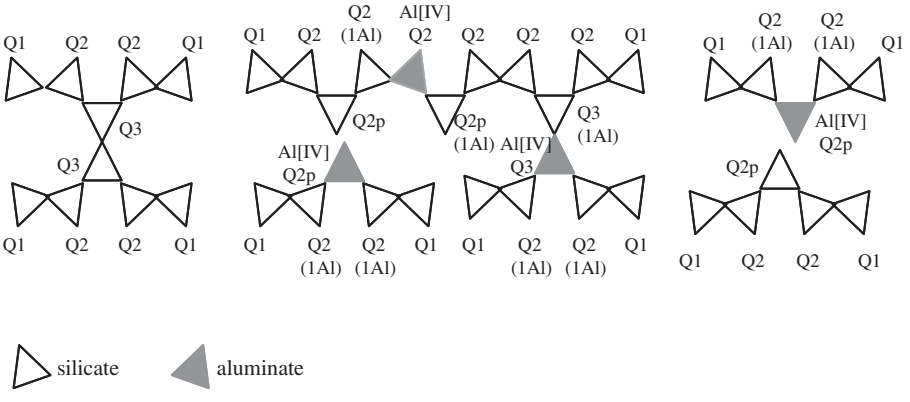

Site	Q_{2p}(1Al)	Q_1	Q_2(1Al)	Q_{2p}	Q_2	Q_3(1Al) + Q_3
δ_{iso} (ppm)	[−77; −76]	[−80; −79]	[−82; −81]	[−83; −82]	[−86; −85]	[−93; −86]

Fig. 8. Schematic representation of finite aluminosilicate chains in a C-A-S-H structure (calcium planes are not shown)—silicate locations and corresponding chemical shifts [45].

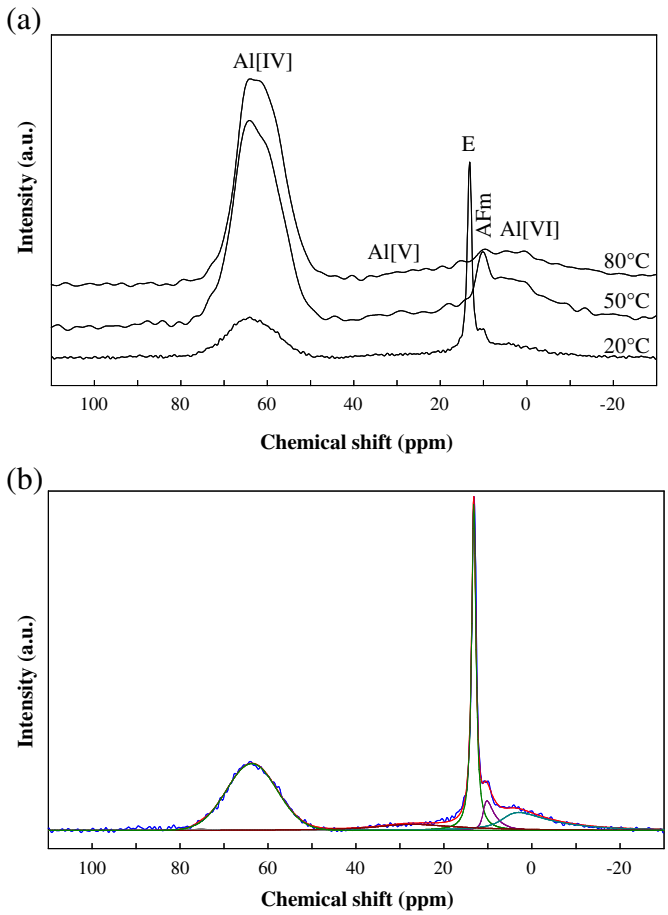

Fig. 9. (a) ^{27}Al MAS NMR spectra for B40 paste after 6 months at 20 °C, 50 °C and 80 °C (Al[IV]: tetrahedral Al; Al[V]: pentahedral Al; Al[VI]: octahedral Al; E = ettringite); (b) example of spectral decomposition for a sample stored at 20 °C.

• B40 paste. The ^{29}Si spectrum for B40 paste versus the curing temperature (Fig. 11) decomposed into 8 components using Gaussian and Lorentzian line shapes (Table 6). The fraction of residual anhydrous phases (C_2S, C_3S) diminished when the curing temperature increased from 20 to 80 °C, resulting in greater progress of hydration as already shown by X-ray diffraction. Raising the temperature from 50 to 80 °C also resulted in a significant drop in the Q_4 signal for silica fume, although SEM observations revealed the presence of residual silica in the paste even at that temperature. It should be noted, however, that all three spectra included a component near −100 ppm, the area of which increased significantly between 50 and 80 °C. This type of chemical shift is characteristic of Si at Q_3 sites in silica fume [53]. Raising the temperature from 50 to 80 °C therefore depolymerized

Table 4
Distribution of aluminum sites (%) in B40 cement paste according to curing temperature (figures in parentheses correspond to fractions calculated with respect to the C-A-S-H sites only).

Chemical shift (ppm)	Line shape used	Assignment of peaks	Temperature (°C)		
			20	50	80
[72–74.1]	Gaussian	C-A-S-H Al(IV) at Q_2 site	<1 (<1)	2 (2)	2
[58.2–64.6]	Gaussian Czjzek model	C-A-S-H Al(IV) at Q_{2p} or Q_3 sites	44 (65)	67 (69)	72
[29–30]	Czjzek model	C-A-S-H Al(V)	8 (12)	5 (5)	5
13.2	Lorentzian	Ettringite	27	0	0
[11.0–11.1]	Czjzek model	AFm	6	3	0
[4.5–5.9]	Czjzek model	C-A-S-H Al(VI)	15 (22)	23 (24)	21
Total C-A-S-H			68	97	100

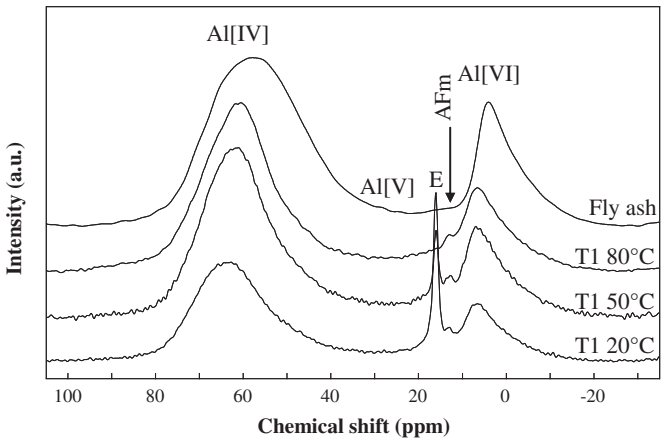

Fig. 10. ^{27}Al MAS NMR spectra for fly-ash and T1 paste after 6 months at 20 °C, 50 °C and 80 °C (Al[IV]: tetrahedral Al; Al[V]: pentahedral Al; Al[VI]: octahedral Al; E = ettringite).

the silica fume by hydrolysis. Moreover, the pozzolanic reaction was enhanced, as evidenced by the reduction in the proportion of silica fume ($Q_3 + Q_4$ sites). The fractions of Q_2(1Al) sites were slightly underestimated with respect to the values calculated from ^{27}Al NMR spectra. The dreierketten structure constraint was satisfied within the uncertainty on the occupancy of the different sites ($[Q_{2p} + Q_3 + Q_3(1Al)]/[Q_2 + Q_2(1Al)] = 0.48$ at 20 °C, 0.50 at 50 °C and 0.51 at 80 °C). Increasing the curing temperature resulted in lengthening (fewer Q_1 sites) and cross-linking (additional Q_3 and Q_3(1Al) sites) of the silicate chains. Lengthening of these chains has already been observed in Portland cement pastes [28]. However, under identical curing conditions, the chain length in these materials is always much shorter than that measured for B40 paste (Q_2/Q_1 ratio for C-A-S-H: 0.8 at 20 °C, 1.3 at 50 °C and 1.7 at 80 °C in Portland cement paste [54], and 4.3 at 20 °C, 6.8 at 50 °C and 24.3 at 80 °C in B40 paste). The fraction of silica fume consumed in B40 paste after six months of curing was assessed from the ^{29}Si NMR spectra: it ranged from 77 to 86% depending on the temperature (Table 7). This fraction was higher than that estimated by Lothenbach et al. [16] on a 1 year-old cement paste of similar composition. In our study, the reactivity of silica fume was improved by the co-grinding treatment applied to the binder before mixing. Our results were however in good agreement with a previous work of Le Saout et al. [55] investigating by ^{29}Si MAS-NMR the pozzolanic activity progress of silica fume in two low permeability cement recipes developed for oil-well cementing. The silica fume to cement ratio was initially equal to 0.24. After 7 months of curing at 20 °C and 10^5 Pa, or 80 °C and 7×10^6 Pa, the fractions of silica fume consumed were 75% and 88% respectively.

Table 5
Estimated silicon fractions at Q_2(1Al) and Q_{2p}(1Al) sites in B40 pastes based on ^{27}Al NMR results.

Sample	B40		
Curing temperature (°C)	20	50	80
Paste mass (g) after end of hydration	10	10	10
Total mass loss by TGA (%)	18.6	17.1	17.0
Cement mass (g)	8.14	8.29	8.30
Al (mmol)	3.289	3.350	3.354
Si (mmol)	70.06	71.35	71.44
Q_{2p}(1Al) sites (%Al)	1	2	2
Q_2(1Al) sites (%Al)	89	136	146
Q_{2p}(1Al) sites (mmol)	3.289×10^{-2}	6.700×10^{-2}	6.708×10^{-2}
Q_2(1Al) sites (mmol)	2.927	4.556	4.897
Q_{2p}(1Al) sites (%Si)[a]	0.05 (±0.05)	0.09 (±0.09)	0.09 (±0.09)
Q_2(1Al) sites (%Si)[a]	4.2 (±0.3)	6.4 (±0.3)	6.9 (±0.3)

[a] Uncertainties calculated assuming the fractions (%) of each site are determined within ±2%.

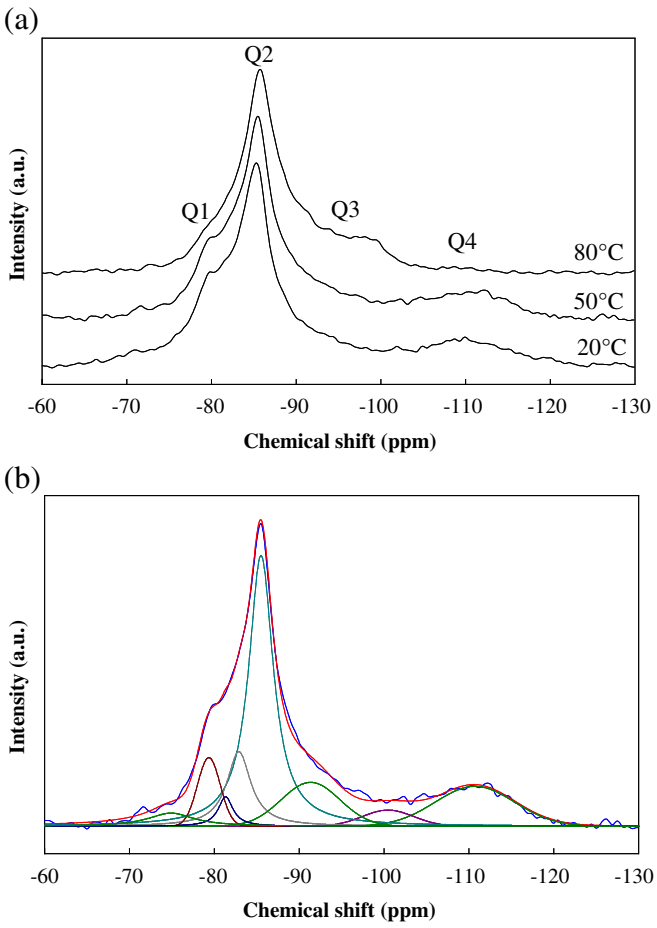

Fig. 11. (a) ^{29}Si MAS NMR spectra for B40 paste after 6 months at 20 °C, 50 °C and 80 °C; (b) example of spectral decomposition for a sample stored at 20 °C.

Using the data provided by ^{29}Si and ^{27}Al NMR, it was also possible to assess the Al/Si ratio in the C-A-S-H, which ranged between 0.04 and 0.06 (Table 7). It should be noted that very similar results were achieved by assuming that the peak at δ~5 ppm on ^{27}Al NMR spectra corresponded to Al[VI] in a distinct phase from C–A–S–H (Al/Si = 0.03 at 20 °C, 0.04 at 50 °C, and 0.04 at 80 °C). The Al/Si ratios calculated from NMR results were in fairly good agreement with those measured by EDS analysis.

- T1 paste: The ^{29}Si spectrum for fly-ash (Fig. 12) had four components that could be identified by their chemical shift: mullite (−88.1 ppm [56]), amorphous silica at Q_3 (−101.9 ppm [53]), amorphous silica at Q_4 (−112.8 ppm [53]), and quartz (−108 ppm [56]). Decomposition of the ^{29}Si NMR spectra for T1 paste was complicated by overlapping of the resonance peaks of the cement hydrates with those of fly-ash and only qualitative analysis was performed (Fig. 13). As for B40 paste, raising the temperature from 50 to 80 °C resulted in silica fume depolymerization: the silica fraction significantly diminished at Q_4 sites, and increased at Q_3 sites. Increasing the curing temperature resulted in lengthening (fewer Q_1 sites) and cross-linking (additional Q_3 sites) of the silicate chains.

Table 6
Distribution of silicon sites (%) in B40 cement paste according to curing temperature (figures in parentheses correspond to fractions calculated with respect to the C-A-S-H sites only).

Shift (ppm)	Assignment of peaks	Temperature (°C)		
		20	50	80
[−73.5; −74.9]	C_2S, C_3S	5	4	1
[−79.2; −79.6]	C–A–S–H Q_1	11 (14)	7 (9)	2 (2)
[−81.0; −81.7]	C–A–S–H Q_2(1Al)	3 (4)	3 (4)	3 (3)
[−82.7; −82.8]	C–A–S–H Q_{2p}	13 (17)	12 (15)	12 (14)
[−85.3; −85.8]	C–A–S–H Q_2	43 (54)	45 (57)	53 (61)
[−90.7; −91.3]	C–A–S–H Q_3(1Al) and Q_3	9 (11)	12 (15)	17 (20)
[−98.1; −100.4]	Silica fume Q_3	3	4	10
[−108.9; −111.1]	Silica fume Q_4	14	14	1
Total C-A-S-H		79	79	87
Total silica fume		17	18	11

Table 7
Effect of curing temperature on residual silica fraction and on Al/Si ratio in C-A-S-H for B40 pastes.

	Sample	B40		
	Curing temperature (°C)	20	50	80
	Paste mass (g) after end of hydration	10	10	10
	Al (mmol)	3.289	3.350	3.354
	Si (mmol)	70.06	71.35	71.44
Silica fume	% of Si sites relative to silica fume	17	18	11
	Residual silica fume (mmol)	11.9	12.8	7.86
	Residual silica fume (g)	0.716	0.772	0.472
	Initial silica fume (g)	3.256	3.316	3.320
	Residual silica fume (%)	22 (±3)	23 (±3)	14 (±3)
C-A-S-H	% of Si sites relative to C-A-S-H	79	79	87
	% of Al sites relative to C-A-S-H	71	98	100
	Si in C-A-S-H (mmol for 10 g sample)	55.3	56.4	62.2
	Al in C-A-S-H (mmol for 10 g sample)	2.34	3.28	3.35
	Al/Si	0.04 (±0.01)	0.06 (±0.01)	0.05 (±0.01)
	Al/Si estimated by EDX	0.04 (±0.01)	0.035 (±0.005)	0.03 (±0.005)

3.2. Effect of temperature on the chemical composition of cement paste pore solutions

The pH of the cement paste pore solutions was assessed by the suspension method (Table 8). Increasing the curing temperature from 20 to 80 °C lowered the cement suspension pH by between 1.8 unit (T1 paste after 3 months) and 2.3 units (B40 paste after 3 months). The pH reduction resulted from the temperature-dependent variation of the activity coefficients (the pK_e of water diminishes from 14.17 at 20 °C to 13.26 at 50 °C and 12.60 at 80 °C), and from silica enrichment of the C-S-H. The pore solution pH varied

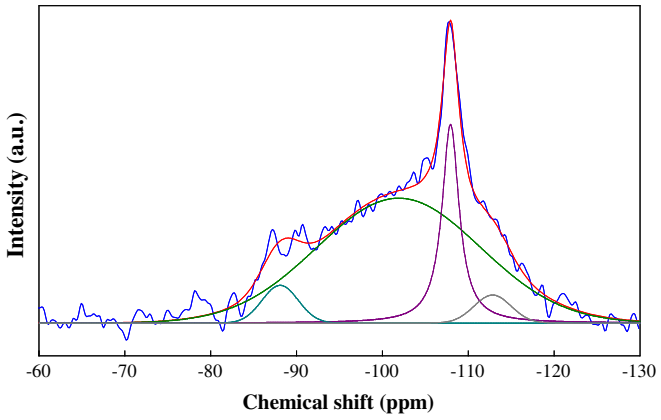

Fig. 12. ^{29}Si MAS NMR spectra for fly-ash.

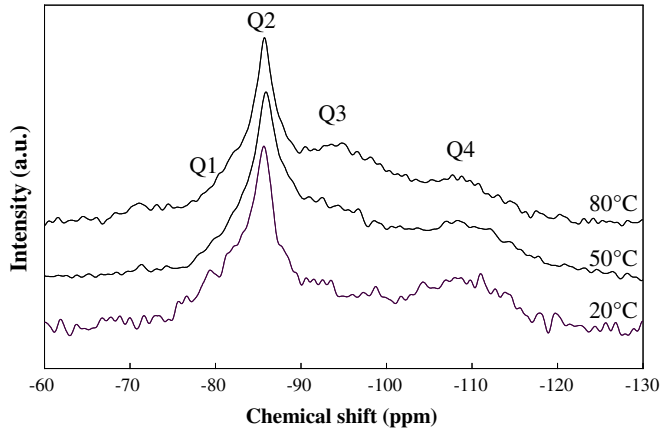

Fig. 13. ^{29}Si MAS NMR spectra for T1 paste after 6 months at 20 °C, 50 °C and 80 °C.

only slightly between 3 and 12 months. Only T1 binder resulted in a pH below 11 at all these temperatures.

The composition of the liquid fraction in the suspensions used to measure the pH was analyzed by ICP-AES (Table 8). The consistency of the results (taking into account all the major species and the measurement accuracy) was estimated by comparing the experimentally measured pH with the value calculated using JChess [57] based only on the experimentally measured Ca, Al, Si, S, Na and K concentrations and the temperature (adjusting the hydroxide ion concentration to ensure electroneutrality). The results obtained using both methods were generally in good agreement, validating the experimental protocol.

Assuming that the solutions were in equilibrium with the phase assemblages, the saturation indexes of the cement phases were calculated from the solution compositions at 20 °C. According to the thermodynamic database used, which contained two C-S-H stoichiometries (C-S-H (1.1) with a Ca/Si ratio of 1.1, and C-S-H (1.8) with a Ca/Si ratio of 1.8) [58,50], the solutions obtained with B40 paste were at equilibrium with ettringite and C-S-H (1.1), which is in good agreement with the experimental results. The T1 paste solutions were slightly over- or undersaturated with respect to ettringite and C-S-H (1.1), but also with respect to gibbsite. The latter phase was not demonstrated experimentally, perhaps because the aluminum was partially inserted in the C-S-H, which was not taken into account by the model.

Raising the curing temperature of B40 and T1 pastes resulted in a sharp increase in the sulfate concentration in solution, as already observed with Portland cement paste [59]. Mineralogical analysis of the solid revealed the disappearance of ettringite from the samples stored at 50 °C and 80 °C and the precipitation of traces of calcium sulfate (gypsum, and possibly anhydrite) after curing for one year. The calculated saturation indexes showed that solutions in contact with B40 and T1 binders after 12 months of curing at 80 °C were oversaturated with respect to anhydrite ($\log \beta = 0.256$ and 0.052 respectively). The solubility of gypsum does not vary significantly with temperature between 25 °C and 90 °C (0.0154 mol/L at 25 °C, 0.0153 mol/L at 45 °C, 0.0146 mol/L at 70 °C, 0.0136 mol/L at 90 °C [60,61]). In contrast, anhydrite exhibits retrograde solubility and becomes more stable than gypsum at temperatures above 40 ± 2 °C [62,63]. The gypsum observed in some samples stored at high temperatures was thus not thermodynamically stable.

The soluble sulfate fraction was always less than 100% (Table 8), even in samples where ettringite degradation was observed without reprecipitation of a sulfate phase. Part of the sulfate therefore remained in the solid phase, probably adsorbed on the C-A-S-H. However, the ability of calcium hydrosilicate to sorb sulfates decreases with their Ca/Si ratio [64], which explains why the sulfate fraction in solution in low pH binder suspensions at 50 and 80 °C is much higher than that obtained under the same conditions with Portland cement (3.1% for a paste hydrated for 6 months at 80 °C [54]).

The concentrations of other ionic species tended to increase more slowly with temperature. This could result mainly from the variation of their activity coefficients which are known to decrease with a temperature increase. Assuming almost constant activities would imply a slight increase in their concentrations.

4. Conclusion

Several conclusions can be drawn after one year of observation of two low pH cement pastes prepared from a binary binder (B40: Portland cement + silica fume) or a ternary binder (T1: Portland cement + silica fume + fly-ash).

(1) The C-A-S-H, which constitutes the main hydrate, was poorly crystallized at the three curing temperatures studied. It was characterized by low Ca/Si ratios (0.75 and 0.85, respectively, for T1 and B40 pastes cured for 6 months at 20 °C, compared with 1.7 for a Portland cement material). The C-A-S-H for T1 paste differed from that of B40 paste by its higher aluminum content (Al/Si ratios of 0.07, compared with 0.04 for B40 binder). The C-A-S-H in B40 and T1 pastes had much longer silicate chains than in Portland cement paste, which is consistent with its lower Ca/Si ratio. Increasing the temperature resulted in a slight reduction in the Ca/Si ratio. At a structural level, lengthening and cross-linking of the C-A-S-H silicate chains were observed.

(2) Ettringite in the pastes stored at 20 °C was destabilized by the temperature rise. The sulfates released were partially adsorbed on C-A-S-H and dissolved in the pore solution. Traces of calcium sulfate (gypsum and anhydrite for B40 paste, gypsum for

Table 8
Composition (concentrations in mmol/L) and pH of the liquid fraction of cement suspensions.

Paste	Curing time (months)	Temp. (°C)	Ca	Si	S	Na	K	Al	Measured pH	Calculated pH	Phases at equilibrium with solution	Fraction of sulfates released in solution (%)
B40	6	20	4.1	1.1	2.7	1.5	0.8	0.01	11.5	11.7	Ettringite $\log \beta = 2.152$ C–S–H(1.1) $\log \beta = 0.161$	15.4
		50	9.2	0.8	9.6	2.5	1.9	0.03	10.3	10.6	–	54.0
		80	9.1	1.5	9.9	2.7	2.4	0.02	9.3	9.9	–	56.1
	12	20	4.0	0.8	2.5	1.4	0.8	0.04	11.5	11.7	Ettringite $\log \beta = 3.39$ C–S–H(1.1) $\log \beta = 0.064$	15.1
		50	8.0	0.8	9.1	2.4	1.9	–	10.2	10.4	–	53.4
		80	10.4	0.7	11.9	2.3	1.6	0.02	9.3	9.3	–	70.4
T1	6	20	3.2	2.1	3.2	1.8	1.1	0.01	11.0	11.0	C–S–H(1.1) $\log \beta = -0.424$ Gibbsite $\log \beta = -0.604$ Ettringite $\log \beta = -0.669$	23.3
		50	6.0	2.0	6.6	2.2	1.4	0.01	10.1	10.1	–	46.0
		80	6.5	3.0	7.4	2.5	1.7	–	9.1	9.3	–	52.1
	12	20	4.2	1.2	4.5	1.9	1.1	0.01	11.1	11.2	Ettringite $\log \beta = 0.678$ C–S–H(1.1) $\log \beta = -0.427$ Gibbsite $\log \beta = -0.733$	33.1
		50	6.8	1.5	7.6	2.1	1.5	–	10.1	10.0	–	54.9
		80	7.1	2.2	8.5	2.5	1.7	–	9.1	9.2	–	60.7

T1 paste) were detected after one year in samples stored at 80 °C (B40 and T1) and 50 °C (B40).

(3) The temperature rise reduced the pore solution pH by about 2 units and caused the sulfate concentration to increase through dissolution of ettringite. Conversely, the soluble alkali fractions did not change significantly.

Hydration remained incomplete in all the materials investigated, even after one year of curing at 80 °C. With regard to the use of these materials in a geological repository, it will be important to determine the final state toward which they could evolve.

Acknowledgments

Xavier Bourbon from ANDRA and Laurent Petit from EDF are deeply acknowledged for their support of this study.

References

[1] B. Lothenbach, K. Scrivener, R.D. Hooton, Supplementary cementitious materials, Cem. Concr. Res. 41 (2011) 1244–1256.
[2] F.P. Glasser, Progress in the immobilization of radioactive waste in cement, Cem. Concr. Res. 22 (1992) 201–216.
[3] F.P. Glasser, Fundamental aspects of cement solidification and stabilization, J. Hazard. Mater. 52 (1997) 151–157.
[4] Proc. 1st Workshop on the Qualification of Low-pH Cement for a Geological Repository, Stockholm, Sweden, October 15–16, 2003, 64 p.
[5] Proc. 2nd Workshop on R&D on Low-pH Cement for a Geological Repository, Madrid, Spain, June 15–16, 2005, 200 p.
[6] Proc. 3 rd Workshop on R&D on Low-pH Cement for a Geological Repository, Paris, France, June 13–14, 2007, 140 p.
[7] M.N. Gray, B.S. Shenton, For better concrete, take out some of the cement, Proc. 6th ACI/CANMET symposium on the durability of concrete, Bangkok, Thailand, May 31 – June 5, 1998.
[8] K. Iriya, A. Matsui, M. Mihara, Study on the applicability of HFSC for radioactive waste repositories, Proc. Radioactive Waste Management and Environmental Remediation, ASME Conference, Nagoya, Japan, September 26–30, 1999.
[9] C. Cau Dit Coumes, S. Courtois, D. Nectoux, S. Leclercq, X. Bourbon, Formulating a low-alkalinity, high-resistance and low-heat concrete for radioactive waste repositories, Cem. Concr. Res. 36 (2006) 2152–2163.
[10] M. Nakayama, K. Iriya, A. Fujishima, M. Mihara, K. Hatanaka, Y. Kurihara, M. Yui, Development of low alkaline cement considering pozzolanic reaction for support system in HLW repository construction, Mater. Res. Soc. Symp. Proc. 932 (2006) 159–166.
[11] M. Codina, C. Cau Dit Coumes, P. Le Bescop, J. Verdier, J.P. Ollivier, Design and characterization of low-heat and low-alkalinity cements, Cem. Concr. Res. 38 (2008) 437–448.
[12] J.L. Garcia Calvo, A. Hidalgo, C. Alonso, L. Fernandez-Luco, Development of low-pH cementitious materials for HLRW repositories—resistance against ground waters aggression, Cem. Concr. Res. 40 (2010) 1290–1297.
[13] S. Hong, F.P. Glasser, Alkali binding in cements pastes. I. The C–S–H phase, Cem. Concr. Res. 32 (2002) 1101–1111.
[14] E.P. Flints, L.S. Wells, Study of the system $CaO-SiO_2-H_2O$ at 30 °C and of the reaction of water on the anhydrous calcium silicates, J. Res. Natl. Bur. Stand. 12 (1934) 751–783.
[15] P.S. Roller, G. Erwin, The system calcium oxide–silica–water at 30 °C—the association of silicate ion in dilute alkaline solution, J. Am. Chem. Soc. 62 (1940) 461–471.
[16] B. Lothenbach, E. Wieland, B. Schwyn, R. Figi, D. Rentsch, Hydration of low-pH cements, Proc. 2nd International Workshop on the mechanisms and modelling of waste/cement interactions, Le Croisic, France October 12 – 16, 2008.
[17] M. Codina, C. Cau Dit Coumes, J. Verdier, P. Le Bescop, J.P. Ollivier, Formulation et caractérisation des bétons bas pH, Rev. Eur. Génie Civ. 11 (2007) 423–435.
[18] T.T.H. Bach, C. Cau Dit Coumes, I. Pochard, A. Nonat, Retention of alkalis by hydrated low-pH cements designed for underground radioactive waste repositories, Proc. 13th International Congress on the Chemistry of Cement, Madrid, Spain, 2011.
[19] ANDRA, Clay report – Evaluating the feasibility of a geological repository in clay formation, ISBN 2-951-0108-8-5 (2005) 238 pp.
[20] M. Pauri, M. Collepardi, Thermo-hygrometrical stability of thaumasite and ettringite, Il Cemento (1989) 177–183.
[21] D. Massiot, F. Fayon, M. Capron, I. King, S. Le Calvé, B. Alonso, J.O. Durand, B. Bujoli, Z. Gan, G. Hoatson, Modelling one and two-dimensional solid-state NMR spectra, Magn. Reson. Chem. 40 (2002) 70–76.
[22] A. Hidalgo, J.L. Garcia, M.C. Cruz, L. Fernadez, L. Fernandez, C. Andrade, Testing methodology for pH determination of cementitious materials—application to low pH binders for use in HLNWR, Proc. 2nd Workshop on R&D on Low-pH Cement for a Geological Repository, Madrid, Spain, June 15–16, 2005.
[23] M. Paul, F.P. Glasser, Impact of prolonged warm (85 °C) moist cure on Portland cement paste, Cem. Concr. Res. 30 (2000) 1869–1877.
[24] F.P. Glasser, M. Tyrer, K. Quillin, D. Ross, J. Pedersen, K. Goldthorpe, D. Bennett, M. Atkins, The chemistry of blended cements and backfills intended for use in radioactive waste disposal, R&D Technical Report P98, Environment Agency, Bristol, Great Britain, 1999, 333 p.
[25] D. Damidot, F.P. Glasser, Thermodynamic investigation of the $CaO-Al_2O_3-CaSO_4-H_2O$ system at 50 °C and 85 °C, Cem. Concr. Res. 22 (1992) 1179–1192.
[26] B. Lothenbach, T. Matschei, G. Möschner, F.P. Glasser, Thermodynamic modelling of the effect of temperature on the hydration and porosity of Portland cement, Cem. Concr. Res. 38 (2008) 1–18.
[27] I. Odler, J. Skalny, Hydration of tricalcium silicate at elevated temperatures, J. Appl. Chem. Biotechnol. 23 (1973) 661–667.
[28] S. Masse, H. Zanni, ^{29}Si solid state NMR study of tricalcium silicate and cement hydration at high temperature, Cem. Concr. Res. 23 (1993) 1169–1177.
[29] A.V. Girao, I.G. Richardson, C.B. Porteneuve, R.M.D. Brydson, Composition, morphology and nanostructure of C–S–H in white Portland cement pastes hydrated at 55 °C, Cem. Concr. Res. 37 (2007) 1571–1582.
[30] A.V. Girao, I.G. Richardson, R.M.D. Brydson, Composition, morphology and nanostructure of C–S–H in white Portland cement—fly ash blends hydrated at 85 °C, Adv. Appl. Ceram. 106 (2007) 283–293.
[31] A.V. Girao, I.G. Richardson, R. Taylor, R.M.D. Brydson, Composition, morphology and nanostructure of C–S–H in white Portland cement—30% fly ash blends hydrated at 55 °C, Cem. Concr. Res. 40 (2010) 1350–1359.
[32] M.D. Andersen, H.J. Jakobsen, J. Skibsted, Incorporation of aluminium in the calcium silicate hydrate (C–S–H) phase of hydrated Portland cements: a high-field ^{27}Al and ^{29}Si MAS NMR investigation, Inorg. Chem. 42 (2003) 2280–2287.
[33] M.D. Andersen, H.J. Jakobsen, J. Skibsted, Characterization of white Portland cement hydration and the C–S–H structure in the presence of sodium aluminate by ^{27}Al and ^{29}Si MAS NMR spectroscopy, Cem. Concr. Res. 34 (2004) 857–868.
[34] M.D. Andersen, H.J. Jakobsen, J. Skibsted, A new aluminum hydrate species in hydrated Portland cements characterized by ^{27}Al and ^{29}Si MAS NMR spectroscopy, Cem. Concr. Res. 36 (2006) 3–17.
[35] F. Brunet, Ph. Bertani, Th. Charpentier, A. Nonat, J. Virlet, Application of ^{29}Si homonuclear and ^{1}H – ^{29}Si heteronuclear NMR correlation to structural studies of calcium silicate hydrates, J. Phys. Chem. B 108 (2004) 15494–15502.
[36] X.C. Cong, R.J. Kirkpatrick, ^{1}H–^{29}Si CPMAS NMR study of the structure of calcium silicate hydrate, Adv. Cem. Res. 7 (1995) 103–111.
[37] P. Faucon, A. Delagrave, J.C. Petit, C. Richet, J.M. Marchand, H. Zanni, Aluminium incorporation in calcium silicate hydrates (C–S–H) depending on their Ca/Si ratio, J. Phys. Chem. B 103 (1999) 7796–7802.
[38] M. Grutzeck, A. Benesi, B. Fanning, Silicon-29 magic angle spinning nuclear magnetic resonance study of calcium silicate hydrates, J. Am. Ceram. Soc. 72 (1989) 665–668.
[39] I. Klur, Étude par RMN de la structure des silicates de calcium hydratés, Ph-D Thesis, Paris VI University, France (1996).
[40] A. Nonat, X. Lecoq, Nuclear magnetic resonance spectroscopy of cement based materials, in: P. Colombet, A.-R. Grimmer, H. Zanni, P. Sozzani (Eds.), Springer Verlag, Berlin, 1998, p. 197.
[41] J. Skibsted, C. Hall, Characterization of cement minerals, cements and their reaction products at the atomic and nano scale, Cem. Concr. Res. 38 (2008) 205–225.
[42] G.K. Sun, J.F. Young, R.J. Kirkpatrick, The role of Al in C–S–H: NMR, XRD, and compositional results for precipitated samples, Cem. Concr. Res. 36 (2006) 18–29.
[43] G. Renaudin, J. Russias, F. Leroux, C. Cau Dit Coumes, F. Frizon, Structural characterization of C–S–H and C–A–S–H samples. Part II: local environment investigated by spectroscopic analyses, J. Solid State Chem. 182 (2009) 3320–3329.
[44] I.G. Richardson, A.R. Brough, R. Brydson, G.W. Groves, C.M. Dobson, Location of Aluminum in Substituted Calcium Silicate Hydrate, C–S–H gels, as determined by ^{29}Si and ^{27}Al NMR and EELS, J. Am. Ceram. Soc. 76 (1993) 2285–2288.
[45] X. Pardal, F. Brunet, T. Charpentier, I. Pochard, A. Nonat, ^{27}Al and ^{29}Si solid-state NMR characterization of calcium alumino-silicate hydrate (C-A-S-H), Inorg. Chem. 51 (2012) 1827–1836.
[46] N.N. Skoblinskaya, K.G. Krasilnikov, Changes in crystal structure of ettringite on dehydration, 1, Cem. Concr. Res. 5 (1975) 381–394.
[47] N.N. Skoblinskaya, K.G. Krasilnikov, Changes in crystal structure of ettringite on dehydration, 2, Cem. Concr. Res. 5 (1975) 419–432.
[48] Q. Zhou, E.E. Lachowski, F.P. Glasser, Metaettringite, a decomposition product of ettringite, Cem. Concr. Res. 34 (2004) 703–710.
[49] J. Skibsted, E. Henderson, H.J. Jakobsen, Characterization of calcium aluminate phases in cement by ^{27}Al MAS NMR spectroscopy, Inorg. Chem. 32 (1993) 1013–1027.
[50] T. Matschei, B. Lothenbach, F.P. Glasser, Thermodynamic properties of Portland cement hydrates in the system $CaO-Al_2O_3-SiO_2-CaSO_4-CaCO_3-H_2O$, Cem. Concr. Res. 37 (2007) 1379–1410.
[51] J.B. D'Espinose de Lacaillerie, C. Fretigny, D. Massiot, MAS NMR spectra of quadrupolar nuclei in disordered solids: the Czjek model, J. Magn. Reson. 192 (2008) 244–251.
[52] G. Engelhardt, D. Michel, High resolution solid state NMR of silicates and zeolites, Wiley, Chichester, United Kingdom, 1987.
[53] K.J.D. MacKenzie, M.E. Smith, Multinuclear solid state NMR of inorganic materials, Materials series, vol. 6, Pergamon, Amsterdam, 2002.
[54] T.T.H. Bach, Évolution physico-chimique des liants bas pH hydratés – influence de la température et mécanisme de rétention des alcalins, PhD thesis, University of Burgundy, France (2010) 236 p.
[55] G. Le Saoût, E. Lécolier, A. Rivereau, H. Zanni, Chemical structure of cement aged at normal and elevated temperatures and pressures. Part II: low permeability class G oilwell cement, Cem. Concr. Res. 36 (2006) 428–433.
[56] H. He, J. Guo, J. Zhu, P. Yuan, C. Hu, ^{29}Si and ^{27}Al MAS NMR spectra of mullites from different kaolinites, Spectrochim. Acta A 60 (2004) 1061–1064.
[57] J. Van der Lee, Thermodynamic and mathematical concepts of CHESS, Technical report LHM/RD/98/39, 1998, p. 99.

[58] E. Revertegat, F. Adenot, C. Richet, L. Wu, F.P. Glasser, D. Damidot, S.A. Stronach, Theoretical and experimental study of degradation mechanisms of cement in the repository environment, Nuclear science and technology, Final report FI2W-CT90-0035, EUR 17642 EN, 1997.
[59] B. Lothenbach, F. Winnefeld, C. Adler, E. Wieland, P. Lunk, Effect of temperature on the pore solution microstructure and hydration products of Portland cement pastes, Cem. Concr. Res. 37 (2007) 483–491.
[60] G.A. Hulett, L.E. Allen, The solubility of gypsum, J. Am. Chem. Soc. 24 (1902) 667–679.
[61] G. Azimi, V.G. Papangelakis, The solubility of gypsum and anhydrite in simulated laterite pressure acid leach solutions up to 250 °C, Hydrometallurgy 102 (2010) 1–13.
[62] E.P. Partridge, A.H. White, The solubility of calcium sulfate from 0 to 200 °C, J. Am. Chem. Soc. 51 (1929) 360–370.
[63] G. Azimi, V.G. Papangelakis, J.E. Dutrizac, Modelling of calcium sulphate solubility in concentrated multi-component sulphate solutions, Fluid Phase Equilib. 260 (2007) 300–315.
[64] R. Barbarulo, H. Peycelon, S. Leclercq, Chemical equilibria between C–S–H and ettringite, at 20 and 85 °C, Cem. Concr. Res. 37 (2007) 1176–1181.
[65] J. Skibsted, H.J. Jakobsen, C. Hall, Direct observation of aluminium guest ions in the silicate phases of cement minerals by ^{27}Al MAS NMR spectroscopy, J. Chem. Soc. Faraday Trans. 90 (1994) 2095–2098.
[66] F. Brunet, T. Charpentier, C.N. Chao, H. Peycelon, A. Nonat, Characterization by solid-state NMR and selective dissolution techniques of anhydrous and hydrated CEM V cement pastes, Cem. Concr. Res. 40 (2010) 208–219.
[67] P. Pena, J.M. Rivas Mercury, A.H. De Aza, X. Turrillas, I. Sobrados, J. Sanz, Solid-state ^{27}Al and ^{29}Si NMR characterization of hydrates formed in calcium aluminate–silica fume mixtures, J. Solid State Chem. 181 (2008) 1744–1752.
[68] J. Schneider, M.A. Cincotto, H. Panepucci, ^{29}Si and ^{27}Al high-resolution NMR characterization of calcium silicate hydrate phases in activated blast-furnace slag pastes, Cem. Concr. Res. 31 (2001) 993–1001.
[69] C.A. Love, I.G. Richardson, A.R. Brough, Composition and Structure of C–S–H in White Portland Cement–20% Metakaolin Pastes Hydrated at 25 °C, Cem. Concr. Res. 37 (2007) 109–117.
[70] S. Murgier, H. Zanni, D. Gouvenot, Blast furnace slag cement: a ^{29}Si and ^{27}Al NMR study, C.R. Chim. 7 (2004) 389–394.